Electronic Supplementary Material (ESI) for Analyst.

Electronic Supplementary Information

Monolayer Detection of Ion Binding at a Crown Ether-functionalised Supramolecular Surface *via* an Integrated Optical Bragg Grating

Richard M. Parker,[a,b] Dominic J. Wales,[a,b] James C. Gates,[b] Jeremy G. Frey,[a] Peter G. R. Smith[b] and Martin C. Grossel*[a]

[a] School of Chemistry, University of Southampton, Highfield, Southampton, United Kingdom, SO17 1BJ

[b] Optoelectronics Research Centre, University of Southampton, Highfield, Southampton, United Kingdom, SO17 1BJ

E-mail: M.C.Grossel@soton.ac.uk

1. EXPERIMENTAL DETAILS

1.1 Equipment and Instrumentation

Melting points were measured using a Gallenkamp Electrothermal melting point apparatus and are uncorrected. Electrospray mass spectra were recorded using a Micromass Platform II single quadrapole mass spectrometer. Nuclear magnetic resonance spectra were collected using a Bruker DPX400 spectrometer; operating at 400 MHz for ^{1}H NMR experiments and 100 MHz for ^{13}C and Dept-135 NMR experiments. ^{13}C NMR spectra were collected fully decoupled. Infrared spectra were collected on a Nicolet 380 FT-IR spectrometer with a SmartOrbit Golden Gate Attenuated Total Reflection (ATR) attachment.

Two-dimensional surface data was collected using a Veeco Thermomicroscopes Explorer non-contact AFM, running Veeco DI SPMlabNT v6.02. Contact angles were calculated for a drop size of 1.0 µL, with a Kruss DSA100 running Drop Shape Analysis (DSA) for windows v1.90.0.14.

Direct UV writing of waveguides was performed using a "Cambridge Laser Laboratories" Lexel 95 SHG UV laser combined with an Aerotech ABL9000 air-bearing stage. Tantalum pentoxide was deposited using an OPT plasmalab 400 Sputter system. Gold was deposited using a BOC Edwards EB3 E-beam linked to a FL400 deposition system. For interrogation at ~1550 nm the waveguide was exposed to an Exfo IQ-2300 erbium fibre-based ASE source as part of an Exfo IQ-203 Optical Test system. The resultant signal was collected by an Ando AQ 6317B optical spectrum analyser (OSA) controlled via a PC running LabVIEW 8.2.1. Fimmwave modelling software is a product of Photon Design and was used as a vectorial mode finder.

Microfluidic pumping was achieved by a Bio-Chem Fluidics solenoid operated micro-pump 130SP1210-1TP, with a 10 µL PTFE chamber, pumping up to 1.2 mL/min. Solutions were switched with a Cole Parmer PTFE manifold mixing solenoid valve, with six inputs leading to one output, capable of transporting 14 L/min at 20 psi. These were connected by Cole Parmer Chemfluor ETFE tubing, with an internal diameter of 0.016" (400 µm) and external diameter of 1/16". Connections were made using Omnifit Omni-Lok Type P fittings, a chemically inert flangeless fitting with a permanently attached PTFE ferrule rated up to 1000 psi.

1.2 Reagents

Commercially available compounds and solvents were obtained from Sigma-Aldrich, Fisher Scientific or Acros Organics and used as supplied without further purification, unless noted. Ethanol and methanol were distilled over calcium sulphate, dichloromethane was distilled over calcium hydride and used immediately. HPLC grade methanol was used as a solvent for Group I binding studies.

2. SYNTHESIS

4'-(Chlorocarbonyl)benzo-15-crown-5 (**3**) was synthesized in three steps from benzo-15-crown-5, each in good yield, as detailed below:

2.1 4'-Acetylbenzo-15-crown-5 (1)[1,2]

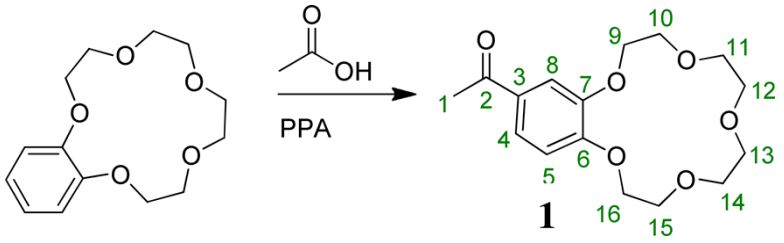

Benzo-15-crown-5 (0.27 g, 1.00 mmol) was dissolved in polyphosphoric acid (6.0 mL) followed by drop-wise addition of acetic acid (0.10 mL, 1.75 mmol) and then was heated for 1.5 hours at 60 ºC. Once complete, the polyphosphoric acid was quenched with water (30 mL) after which the product was extracted into chloroform (3x40 mL), the combined extracts were dried and the solvent was removed *in vacuo* to give a white solid (**1**) (0.32 g, >99 %). MP: 93 – 94 ºC (Lit:[1] 94-95 ºC). ^{1}H NMR ($CDCl_3$): 2.55 (s, 3H, H_1), 3.77 (d, J=2.8 Hz, 8H, $H_{11\text{-}14}$), 3.93 (ddd, J=8.4, 4.4, 4.3 Hz, 4H, $H_{10,15}$), 4.20 (dd, J=4.4, 3.1 Hz, 4H, $H_{9,16}$), 6.86 (d, J=8.3 Hz, 1H, H_5), 7.51 (d, J=2.0 Hz, 1H, H_8), 7.56 (dd, J=8.5, 2.0 Hz, 1H, H_4). ^{13}C NMR ($CDCl_3$): 26.2 (C1), 68.7 – 69.4 ($C_{11\text{-}14}$), 70.4 (C_{15}), 70.4 (C_{10}), 71.2 ($C_{9,16}$), 111.8 (C_8), 112.8 (C_5), 123.5 (C_4), 130.7 (C_3), 148.8 (C_7), 153.5 (C_6), 196.7 (C_2). IR (v/cm^{-1}): 2962 (C-H aromatic), 2906, 2858 (C-H alkyl), 1666 (C=O), 1593, 1582 (C=C aromatic), 1012 (C-O). MS (ES$^+$, MeCN, m/z): 311 (5.5 %, $[M+H]^+$), 328 (8.2 %, $[M+NH_4]^+$), 333 (100.0 %, $[M+Na]^+$), 349 (2.4 %, $[M+K]^+$).

2.2 4'-Carboxybenzo-15-crown-5 (2)[1,3]

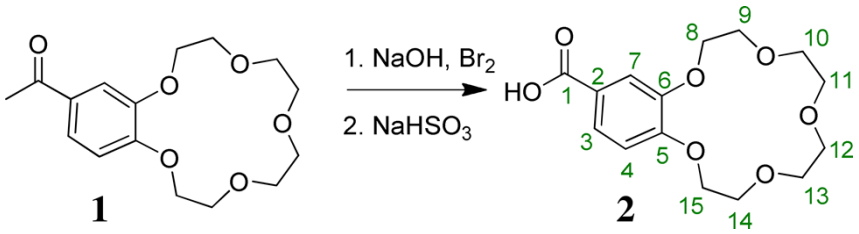

To a stirred solution of sodium hydroxide (2.65 g, 66.3 mmol) in water (19 mL) maintained below 10 ºC, bromine (0.20 mL, 3.90 mmol) was added drop-wise. 4'-Acetylbenzo-15-crown-5 (**1**, 0.29 g, 0.919 mmol) was then added with vigorous stirring. After 4 hours, sodium bisulphite (1.12 g, 9.33 mmol) was added to quench the reaction mixture which resulted in immediate decolourisation. The reaction mixture was filtered, washed with chloroform (3 x 25 mL) and acidified to pH 3 (conc. HCl, <8 mL). The aqueous mixture was subsequently extracted with dichloromethane (3 x 25 mL). The combined extracts were dried over magnesium sulphate and the solvent removed *in vacuo* to give a white solid (**2**) which was crystallised from ethanol (0.27 g, 94 %). MP: 185.0 – 185.5 ºC (Lit:[1] 185-186 ºC). ^{1}H NMR ($CDCl_3$): 3.62 (s, 8H, $H_{10\text{-}13}$), 3.69 - 3.86 (m, 4H, $H_{9,14}$), 4.09 (ddd, J=9.0, 4.4, 4Hz, 4H, $H_{8,15}$), 7.02 (d, J=8.6 Hz, 1H, H_4), 7.43 (d, J=2.0 Hz, 1H, H_7), 7.55 (dd, J=8.4, 1.8 Hz, 1H, H_3), 12.68 (br. s., 1H, H_{acid}). ^{13}C NMR ($CDCl_3$): 68.3 – 68.8 ($C_{10\text{-}13}$), 69.6 (C_{14}), 69.7 (C_9), 70.5 – 70.6 ($C_{8,15}$), 112.3 (C_4), 113.8 (C_7), 123.1 (C_3), 123.4 (C_2), 147.9 (C_6), 152.4 (C_5), 167.0 (C_1). IR (*v*/cm^{-1}): 2930 (C-H aromatic), 2854 (C-H alkyl), 1668 (C=O), 1587, 1582 (C=C aromatic), 1053 (C-O). MS (ES$^+$, MeOH, m/z): 330 (3.9 %, $[M+NH_4]^+$), 335 (100.0 %, $[M+Na]^+$), 349 (1.3 %, $[M+K]^+$). MS (ES$^-$, MeOH, m/z): 311 (100.0 %, $[M-H]^-$).

2.3 4'-(Chlorocarbonyl)benzo-15-crown-5 (3)[4]

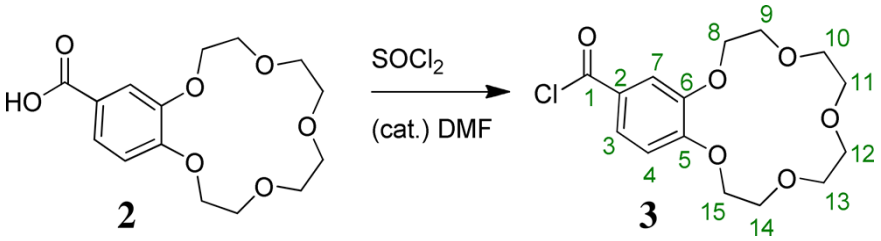

4'-Carboxybenzo-15-crown-5 (**2**, 0.0512 g, 0.164 mmol) was refluxed in thionyl chloride (5.0 mL, 68.5 mmol) containing several drops of catalytic dimethylformamide for 24 hours under nitrogen. The remaining thionyl chloride was removed by distillation under vacuum (50 ºC), before drying the cream residue (**3**). This was assumed to be a quantitative conversion and the product was used immediately without further purification. MS (ES^+, MeCN, m/z): 331 (51.3 %, $[M+H]^+$), 353 (6.5 %, $[M+Na]^+$), 369 (1.6 %, $[M+K]^+$). MS (ES^+, MeOH, m/z): 331 (7.5 %, $[M+H]^+$), 330 (3.9 %, $[M+NH_4]^+$), 353 (4.6 %, $[M+Na]^+$), 369 (3.1 %, [M+K]+). 335 (51.1 %, $[N+Na]^+$), 349 (18.4 %, $[N+K]^+$). MS (ES^-, MeOH, m/z): 311 (61.9 %, $[N-H]^-$), not seen in MeCN ES^- samples). N represents the molecular ion for 4'-carboxybenzo-15-crown-5 (13). While mass spectrometry samples in acetonitrile shows only the acid chloride, those collected in methanol show decomposition back to the carboxylic acid. The methyl ester was not detected.

3. SURFACE MODIFICATION

3.1 Adhesion to Tantalum pentoxide

The inclusion of a thin film of tantalum pentoxide on the sensor surface was previously introduced as a method of increasing the sensitivity to refractive index change.[5] It has been reported that the hydroxyl surface of the tantalum pentoxide film allows for it to be functionalized analogously to silica.[6] This was confirmed by the attachment of a layer of (3-mercaptopropyl)trimethoxysilane to a freshly cleaned surface, before the subsequent deposition of a 50 nm gold film. Gold is known to attach to thiols but will not adhere strongly to silica or tantalum pentoxide surfaces, allowing for functionalized regions to be differentiated [7]. Adhesion tests demonstrated that untreated surfaces retained no gold, while both the silica and tantalum pentoxide-functionalized surfaces retained complete gold films (Figure S1).

Procedure:

The sample surface was cleaned in "piranha solution" (4 mL) for 15 minutes after which it was rinsed in water and transferred to a solution of NH_4OH:H_2O_2:H_2O (1:1:4, 3 mL) for a further 15 minutes. The sample was then thoroughly washed with water. (3-Mercaptopropyl)trimethoxysilane (5 mL) was refluxed in a mixture of isopropanol and water (40:1, 205 mL). Into this mixture was suspended the freshly cleaned surface for 10 minutes, after which it was removed, rinsed with isopropanol and baked for 10 minutes at ~100 °C. This procedure was repeated a further two times before the surface was finally washed vigorously with isopropanol. Gold was deposited onto the functionalised surface to a depth of 50 nm. Adhesion was tested using cellulose tape:

Adhesion:	Silica	– 100 %	(untreated silica – 0 %)
	Tantalum pentoxide	– 100 %	

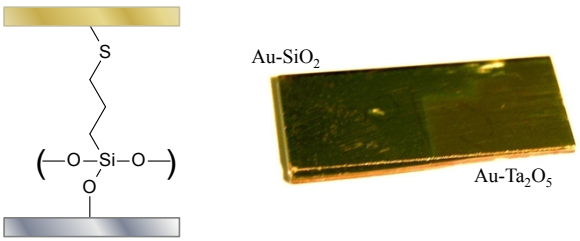

Fig. S1 Successful adhesion of gold to both glass and tantalum pentoxide surfaces *via* a (3-mercaptopropyl)trimethoxysilane bridge, as shown schematically (left).

3.2 Deposition of a self-assembled monolayer of (3-aminopropyl)triethoxysilane

The functionalisation of the sensor surface within the microchannel consisted of cleaning and preparative steps, followed by chemical reaction and optical calibration against a known reference solution. Within the microfluidic flow cell each of these individual steps can be concatenated into a single, automated recipe that was applied sequentially to the microreactor. The pump period and the switching of reservoirs was controlled using a custom LabVIEW script connected *via* a USB DAQ controller. Each of the five stock solutions were freshly prepared and connected to a separate inlet to the microfluidic system (see Figure S7) and air bubbles cleared from the tubing. By switching the six-way valve, solutions were then selectively drawn through the microreactor and over the sensor surface, as given by the following recipe. A constant pump period was used throughout the experiment of 3.0 s, corresponding to a pump rate of 0.2 mL/min. This was a continuous process and was conducted as a single experiment, monitored in real-time *via* the Bragg grating (see Figure 1).

The typical recipe used to clean and functionalise the surface was as follows:

1)	deionised water	30 minutes
2)	acetone	30 minutes
3)	deionised water	30 minutes
4)	potassium hydroxide (5.0 M)	60 minutes
5)	deionised water	20 minutes
6)	methanol/ethanol (reference)	80 minutes
7)	10 % 3-APTES in methanol/ethanol	720 minutes
8)	methanol/ethanol (reference)	80 minutes

The two alcohol washes were used as a comparative reference, allowing for the change in the effective index of the waveguide to be calculated upon surface functionalisation with 3-APTES. An ethanol reference was used throughout the confirmatory experiments and in modelling, however methanol was the solvent choice for the crown ether experiments where the thicker tantalum pentoxide layer reduced the dynamic range of the Bragg sensor (Figure S6).

3.2 Attachment of fluorescein isothiocyanate to a 3-APTES monolayer surface

An analogous procedure was followed for the attachment of fluorescein isothiocyanate (FITC) to the 3-APTES monolayer surface, with the pump period kept constant at 3.0 s. While the six-way valve would have allowed for this step to be carried out as part of the previous recipe as a single process, the potential for FITC to hydrolyse during the 18.8 hours of process prior to flowing over the microreactor was considered an issue. The following recipe was employed:

1)	methanol (reference)	80 minutes
2)	FITC in DMSO (20mg in 150 mL)	720 minutes
3)	methanol (reference)	80 minutes

Functionalisation of the surface with FITC was interrogated by the change in the Bragg wavelength between the two methanol reference flows, compared to the modelled result and independently verified by fluorescence microscopy.

3.3 Attachment of 4'-(chlorocarbonyl)benzo-15-crown-5 (3) to a 3-APTES monolayer surface

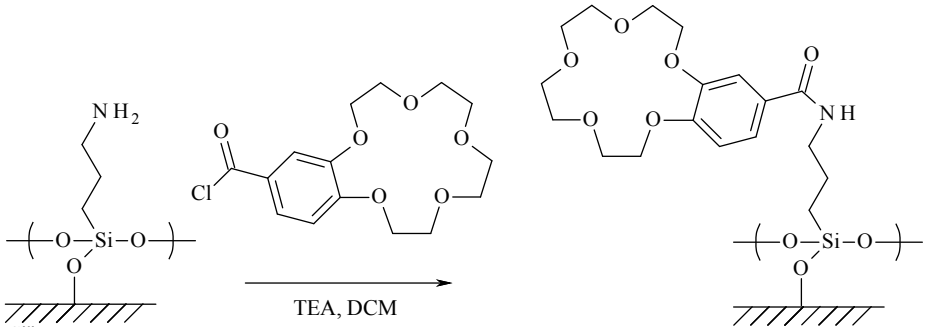

A large excess of **3** (~ 50 mg) was dissolved in dichloromethane (80 mL), to this was added triethylamine (<0.01 mL). The 3-APTES modified surface, mounted within the microfluidic flow cell was then sequentially exposed to the following solutions:

4) methanol (reference) 80 minutes
5) 4'-(chlorocarbonyl)benzo-15-crown-5 solution (DCM) 720 minutes
6) methanol (reference) 80 minutes

To reduce the amount of **3** consumed per experiment, a lower pump period was used of 6.0 s, corresponding to a pump rate of 0.1 mL/min throughout the three steps. The success of the surface functionalisation was interrogated by the change in the Bragg wavelength between the two methanol reference flows.

Figure S2 plots the Bragg wavelength shift during the attachment of **3** to the 3-APTES surface as detailed above, illustrating the increase in Bragg wavelength after attachment. In contrast, where the procedure to attach **3** onto the sensor was repeated in the absence of a 3-APTES monolayer, no increase in Bragg wavelength was observed. Similarly flowing only solvents over the surface did not give rise to a permanent Bragg wavelength shift. These control experiments, combined with the evidence given for the presence of a viable 3-APTES monolayer and the use of standard attachment chemistry is presented as evidence that this Bragg wavelength increase is exclusively the result of **3** bonding to the 3-APTES monolayer surface. Interestingly, attachment of both small, aromatic molecules, FITC and **3**, were observed to give a ~9x greater Bragg wavelength shift than observed for the corresponding attachment of 3-APTES. While ellipsometry of the surface was attempted, reflections from the layered glass structure masked any measured signal. As noted in Section 4.4, without a reasonable estimate of the refractive index of **3,** modelling of its attachment to the 3-APTES surface is not presented as corroboration of the Bragg wavelength shift observed. It should be further commented that unlike FITC, **3** is not fluorescent and is also not significantly more lipophilic than 3-APTES to give a markedly different contact angle, making these methods of verification unsuitable.

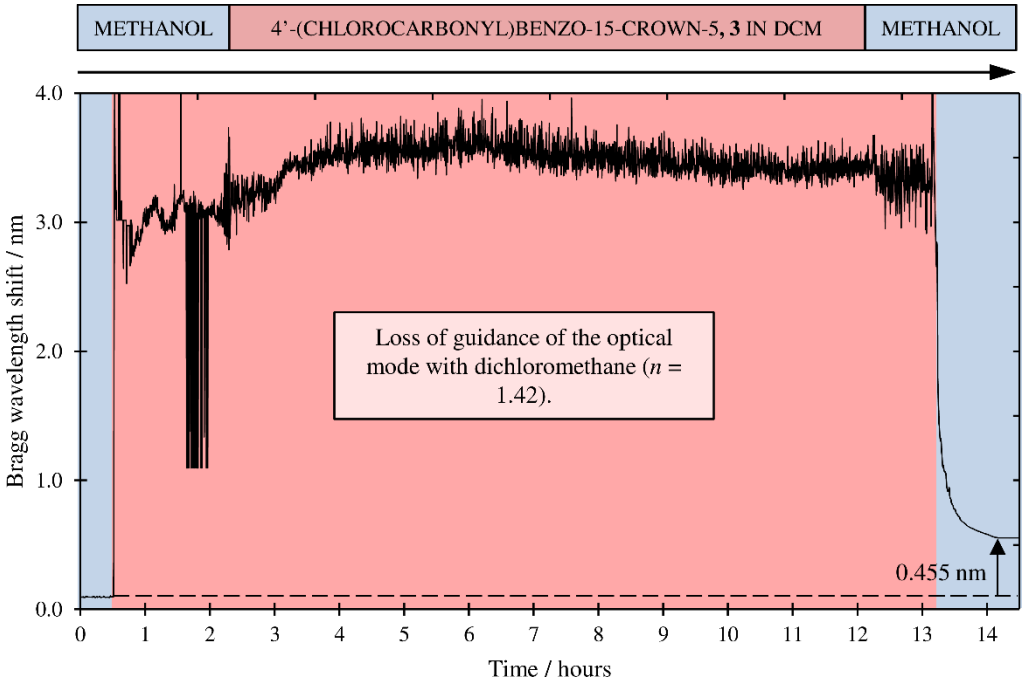

Fig. S2 The average Bragg wavelength shift for the three sensor Bragg gratings during the attachment of 4'-(chlorocarboxy)benzo-15-crown-5, **3** to the preformed 3-APTES SAM sensor surface. A difference of 455 pm was recorded between the two methanol reference flows due to the attachment of **3**. The high refractive index of the dichloromethane reaction solvent resulted in temporary loss of optical guidance (see Figure S6), preventing the direct Bragg wavelength shift during reaction from being recorded in an analogous manner to Figure 1.

3.4 Coordination of Group (I) salts to the crown ether monolayer surface

To probe the ability of the Bragg sensor to detect binding to the crown ether-functionalised monolayer surface a series of solutions ranging from 1.0 µM to 10 mM in methanol were prepared by serial dilution of LiBr, NaCl, KCl and RbCl stock solutions. Using the automated microfluidic system, each solution was flowed over the surface for 80 minutes with a pump period of 0.5 s, corresponding to 1.2 mL/min. This was followed by an 80 minute wash with pure methanol to restore the surface, before repeating the process. Each solution was flowed over the sensor a total of three times and the average Bragg wavelength shifts reported in Figure 5.a.

4. INTEGRATED OPTICAL BRAGG GRATING REFRACTOMETER

4.1 Fabrication

One route to fabricate a wide range of integrated optical devices is the process of direct UV writing [13]. This technique is based on the local refractive index increase of a photosensitive planar glass layer through exposure to a tightly focused UV-laser beam. The translation of this beam relative to the substrate allows for the definition of two-dimensional waveguiding structures; from splitters and couplers to Mach-Zehnder interferometers, without the need for photolithographic or subsequent processing. Through a further modification to this technique, Bragg gratings (an optical component that acts as a wavelength-selective reflector) can be simultaneously incorporated directly into the waveguide. Fabrication is achieved by generating a periodic intensity pattern at the focal point of two interfering UV laser beams. By controlling the modulation of this interference pattern, the form of the grating can be precisely controlled. By altering the period of this modulation multiple gratings can be written over a wide wavelength range within a single waveguide channel.

For this work, a three-layer planar glass structure was fabricated on to a silicon substrate by flame hydrolysis deposition (CIP, Ipswich, UK), comprising of undercladding, core and overcladding layers with a total silica layer thickness of ~40 µm. The 6 µm thick core layer was doped with germanium to raise its refractive index above that of the cladding and to also introduce photosensitivity. The dimensions of this planar device was 10.0 x 20.0 mm.

The waveguiding structure was UV-written into the core layer of this planar glass structure, with its dimensions defined by the thickness of the core layer and the width of the focal point of the interfering UV laser beam (giving rise to a cross-section of approx. 6 x 6 µm). When the device was translated through the UV beams a channel waveguide was written, however, through controlled modulation of this interference pattern Bragg gratings can also be formed selectively along the waveguide. Precise control of this modulation of the laser intensity during fabrication of the periodic grating structure results in an apodised Bragg grating (i.e. the gratings fringe visibility changes with position). In this work the intensity profile of the modulated Bragg grating structure was defined by a Gaussian envelope, giving rise to Gaussian apodised Bragg peaks in the reflected spectrum (as discussed later and in Figure S5). Four Bragg gratings were written into a single waveguiding channel, each Bragg grating being 2 mm long and with a period between 529 and 542 nm, satisfying the Bragg condition (Eqn S1) to reflect at wavelengths between 1530 and 1570 nm. A schematic of a typical device is shown in Figure S3.

A commercial polarisation maintaining (PM) optical fibre 'pigtail' was aligned and robustly attached to the integrated Bragg grating device *via* a commercially available 'v-groove' optical fibre assembly and an optical grade UV-cured adhesive, with less than 0.2 dB insertion loss. This allows for the sensor device to be connected to the optical interrogation system by standard PC or APC optical fibre connections (see Figure S4).

To access the evanescent mode of the waveguide a micro-channel was etched into the overclad with hydrofluoric acid/hydrochloric acid (4:3:9 HF:HCl:H_2O), with real-time feedback (final etch depth: 18 µm, $\Delta\lambda_B$ = 1.2 nm). The surface of the etched well was mechanically polished with an alkali, colloidal silica solution (SF1) for 20 – 30 seconds. This was instantly washed with copious amounts of deionised water and dried. Finally, tantalum pentoxide (~ 50 nm) was sputtered over the etched region. Through comparison before and after sputter deposition, it was observed that the Bragg gratings increased in amplitude while the Bragg wavelength shifted to higher wavelength. The etched sensor was calibrated against a

series of reference Cargille refractive index liquids (Series AA and AAA), both before and after deposition of tantalum pentoxide, as exemplified in Figure 2a the presence of this thin-film of high-index material dramatically increases the sensitivity of the device.

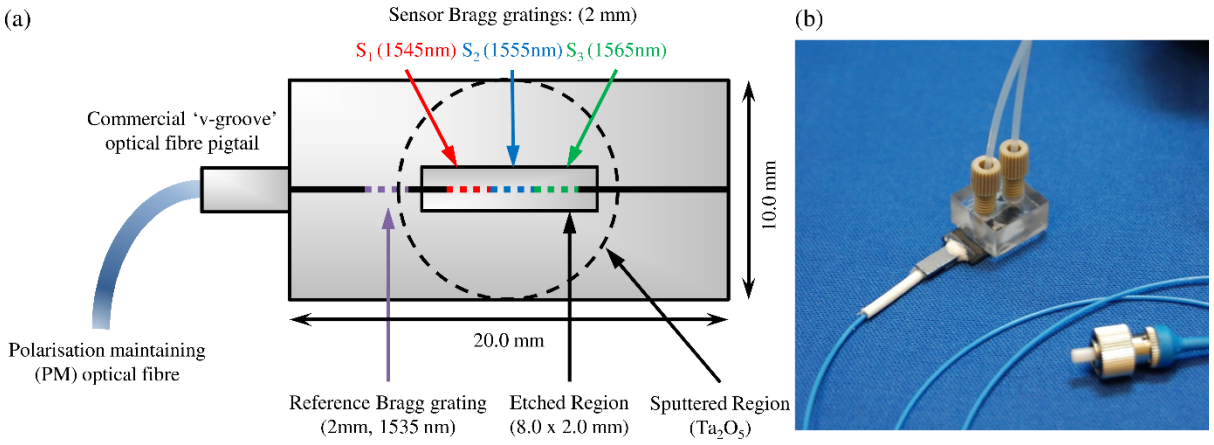

Fig. S3.(a) A schematic of the UV-written, etched and fibre coupled Bragg grating sensor, showing the position and Bragg wavelengths of the Bragg gratings within the sensor window. Sensor Bragg gratings were adjacent along the waveguide. **(b)** A photograph of a prototype microfluidic device fabricated from Perspex, allowing the assembled integrated optical sensor and fibre pigtail to be visualised within.

4.2 Detection

A broadband Amplified Spontaneous Emission (ASE) source was used to analyse the sensor. This was linked by optical fibre to a polarisation maintaining (PM) polariser. The PM polariser was used to polarise the input light to an orientation aligned to one of the principle axes of the PM fibre with a suppression of orthogonal polarisation mode of 30 dB (1000:1). From this point the signal is transmitted through PM fibre, minimising changes in polarisation from movement of the fibre during measurements. This is necessary as the peak wavelength of the transverse magnetic (TM) and transverse electric (TE) modes are different and any switch between will produce an anomalous shift in the sensor output. For the purposes of these experiments the TE mode was selected as this had previously been shown through modelling (*Fimmwave*) to have a higher sensitivity in the presence of a high-index overlayer. The circulator allows the reflected signal to be directed to the optical

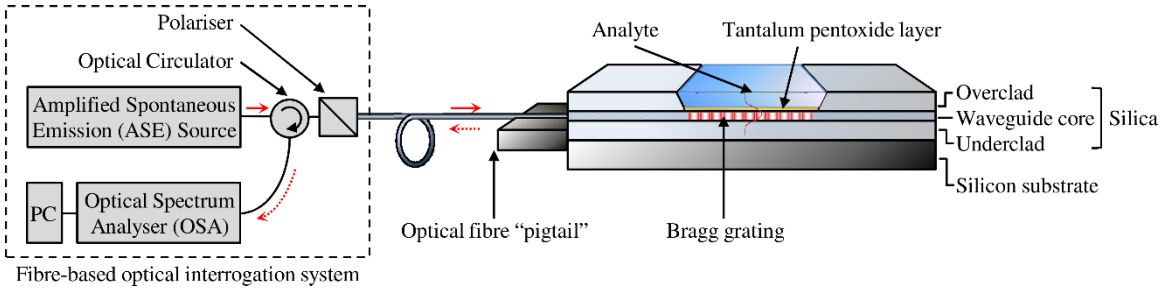

spectrum analyser (OSA) which was controlled remotely, via a PC running LabVIEW (Figure S4).

Fig. S4. A schematic of an etched and fibre coupled Bragg grating sensor, showing the exposed Bragg grating within the window. The readout system is connected to the chip using standard optical fibre and is robustly pigtailed using standard telecomm assembly techniques.

Each Bragg grating will reflect a characteristic Bragg peak at a wavelength (λ_B) dependent on its local refractive index and grating period (Figure S5), as given by the Bragg condition:

$$\lambda_B = 2n_{eff}.\Lambda \qquad \text{(Eqn. S1)}$$

where n_{eff} is the effective refractive index of the Bragg grating (i.e. the average refractive index experienced by the optical guided mode) and Λ is the period of the refractive index modulation of the grating structure. The spectral shape of the reflected Bragg peak is dictated by any deviation from a uniformly periodic grating structure; in this work this was

modulated to result in the reflected peak describing a Gaussian apodised profile. It should also be noted that the high sensitivity to refractive index reported in this work is only possible through the high spectral fidelity of these Gaussian-apodised Bragg gratings.

This Bragg wavelength can be determined from the reflected spectrum, which in this work focuses upon the telecommunication wavelengths (1530-1570 nm). To extract this information, a custom LabVIEW program was written to spectrally identify and fit a Gaussian profile to each reflected Bragg peak. From the equation of the fitted Gaussian the central Bragg wavelength (λ_B) could be determined and its shift with changes in refractive index tracked with time. As this is an absolute measurement of a physical property it does not require continued monitoring and can be compared between experiments, however it should be noted that n_{eff} (and λ_B) is presented in this work as a shift relative to an initial value, i.e. Δn_{eff}, and $\Delta\lambda_B$, rather than as an absolute refractive index.

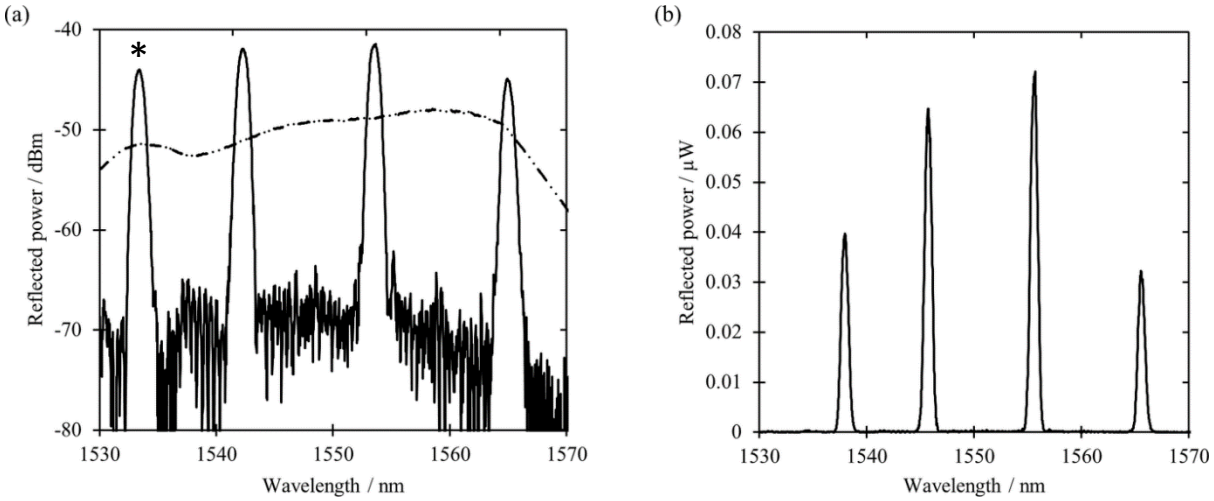

Fig. S5 The device consisted of four spectrally distinct Bragg gratings, one un-etched reference (*, ~1535nm) and three sensor gratings distributed along a linear waveguide. The reflected spectrum of the integrated optical device is plotted both **(a)** logarithmically and **(b)** linearly, showing the Gaussian profile of the Bragg peaks and low optical noise. The dashed line in (a) represents the 4 % reflection from the optical fibre interrogation system alone and it is this profile that leads to the variation in peak height in (b).

The sensitivity of the Bragg grating is dependent on the magnitude of the optical mode that evanescently propagates within the analyte. This can be controlled by adjusting the thickness of the thin film of high-index, tantalum pentxide, as shown in Figure S6. This process is self-amplifying as the analyte approaches the index of the waveguide core (1.45), resulting in a non-linear sensitivity curve. For highly sensitive devices, i.e. larger thicknesses, the refractive index cut-off of the analyte (at which the guided optical mode is lost completely into the analyte) is much lower, leading to reduced dynamic range.

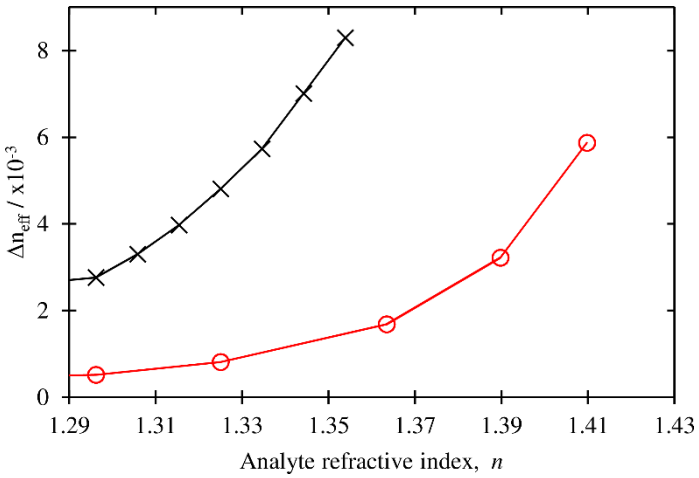

Fig S6 A comparison of effective refractive index of the transverse electric optical mode of the waveguide for increasing analyte refractive index for the integrated optical Bragg grating sensors coated with a thin film of tantalum pentoxide of 47 nm (**o**) and 72 nm (**X**) in thickness. For the thicker layer, guidance of the optical mode is lost at a lower analyte refractive index.

4.3 Microfluidic flow cell

The microfluidic flow cell was milled from stainless steel and sealed on top of the planar optical device with a Kalrez O-ring, this was found to be resilient to common solvents, acids and base.[8] Fluid flow was controlled by a PTFE diaphragm pump upstream of the flow cell. To select the desired reagent, a PC-controlled six-way PTFE diaphragm valve was incorporated into the system and connected *via* 400 µm bore ETFE tubing (Figure S7). The specification of the components

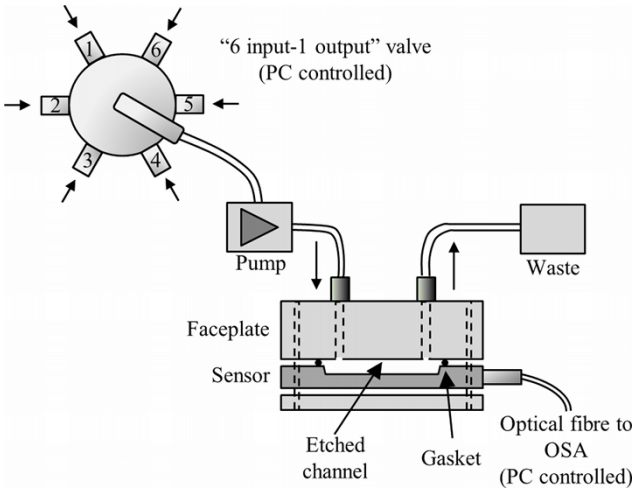

used can be found in Section 1.1.

Fig. S7 A schematic of the microfluidic setup.

4.4 The modelled waveguide

The waveguide modes were numerically solved using the commercial mode solving package *Fimmwave* (Photon Design), which is based upon a Film Mode Matching method. This fully vectorial mode solver inherently sub-divides the waveguide geometry into areas of refractive index chunks, allowing for reduced calculation complexity. This subdivision occurs by splitting up the geometry into a sandwich of vertical slices each considered to be cut from a slab waveguide. Subsequent to subdivision of the waveguide, the supported modes of the defined structure are obtained by the algorithm by collecting the modes that have the same wavevector along the propagation dimension and matching the field distributions at the slice interfaces by adjusting the modal amplitudes in each slab. Once the guided optical mode profile has been modelled, the

effective refractive index of the waveguide can be determined and plotted as a function of varying a parameter of the waveguide structure. This approach has been employed previously by the authors to model thin-film growth.[5]

To fully model the waveguide in this work, the cross-section of the integrated optical waveguide was represented as shown in Figure S8, with the intensity profile of the transverse electric guided mode included here for visual reference. Accurate modelling of the optical mode of the waveguide is highly dependent on the thickness and refractive index of each of these layers.

The refractive index of the underclad (n = 1.4446) and the doped layer (1.4465) containing the UV-written waveguide core (1.4515) were dictated by the FHD process. The thickness of the core, post etching of the overclad, was determined by measuring the etched depth and calibrated against the sensitivity of the etched sensor to a series of Cargille refractive index liquids (Series AA and AAA). After deposition of a thin-film of tantalum pentoxide, the device was calibrated a second time to allow the precise refractive index (2.1200) and thickness of this layer to be modelled (Fig. 2a).

To represent the deposition of the self-assembled monolayer within the microchannel, an effectively infinite layer of ethanol (1.3500) was modelled above the surface and the effect on the effective index of the guided mode of depositing a thin film (0 –50 nm) of either refractive index 1.4400 or 1.7400 (for 3-APTES and FITC-APTES respectively) was then calculated using *Fimmwave*. It should be noted that as shown by Figure S6, the absolute sensitivity of the waveguide ($\Delta\lambda_B/\Delta n$) is dependent on the refractive index of the analyte; as such it is imperative to model the deposition of the monolayer in the presence of the appropriate solvent.

We were unable to find a reasonable estimate of the refractive index of 4'-carboxybenzo-15-crown-5 and hypothesise that the refractive index of the crown ether is likely to vary dramatically between the solid state, in solution or as a solvated monolayer. Further, the refractive index of the layer is likely to vary depending on the confirmation and contents of the of the macrocyclic cavity. As such modelling of the attachment of **3** to the APTES surface and subsequent surface binding events are not presented in this work.

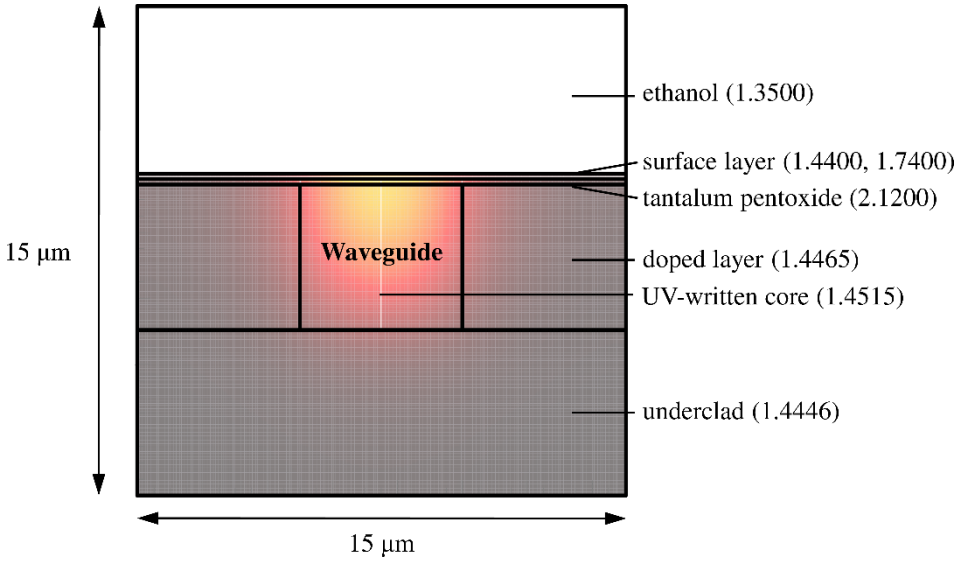

Fig. S8 The modelled cross-section of the waveguide for the TE guided mode, showing the high-index overlayer and organic monolayer on the waveguide surface, in ethanol.

REFERENCES

1. V. Percec, G. Johansson, J. Heck, G. Ungarb, and S. V Batty, *J. Chem. Soc. Perkin Trans. 1*, 1993, 1411–1420.
2. M. Tada, H. Hamazaki, and H. Hirano, *Bull. Chem. Soc. Japan*, 1982, **55**, 3865–3869.
3. M. Bourgin, K. H. Wong, J. Y. Hui, and J. Smid, *J. Am. Chem. Soc.*, 1975, **97**, 3462–3467.

4. L. H. Uppadine, J. E. Redman, S. W. Dent, M. G. B. Drew, and P. D. Beer, *Inorg. Chem.*, 2001, **40**, 2860–2869.
5. R. M. Parker, J. C. Gates, M. C. Grossel, and P. G. R. Smith, *Appl. Phys. Lett.*, 2009, **95**, 173306.
6. R. De Palma, W. Laureyn, F. Frederix, K. Bonroy, J.-J. Pireaux, G. Borghs, and G. Maes, *Langmuir*, 2007, **23**, 443–451.
7. C. A. Goss, D. H. Charych, and M. Majda, *Anal. Chem.*, 1991, **63**, 85–88.
8. R. M. Parker, J. C. Gates, D. J. Wales, P. G. R. Smith, and M. C. Grossel, *Lab Chip*, 2013, **13**, 377–385.